


RESEARCH ARTICLE

Representative general circulation models selection and downscaling of climate data for the transboundary Koshi river basin in China and Nepal

Santosh Kaini^{1,2}  | Santosh Nepal³ | Saurav Pradhananga³ | Ted Gardner¹ | Ashok K. Sharma¹

¹Victoria University, College of Engineering and Science, Melbourne, Victoria, Australia

²Ministry of Energy, Water Resources and Irrigation, Kathmandu, Nepal

³International Centre for Integrated Mountain Development (ICIMOD), Kathmandu, Nepal

Correspondence

Santosh Kaini, Victoria University, College of Engineering and Science, Footscray Park Campus, ISILC, POBox 14428, Melbourne, Vic 8001, Australia
Email: santosh.kaini@live.vu.edu.au

Ashok K. Sharma, Victoria University, College of Engineering and Science, Footscray Park Campus, ISILC, POBox 14428, Melbourne 8001, Australia.
Email: ashok.sharma@vu.edu.au

Abstract

The selection of general circulation models (GCMs) with high capability to represent the past and likely future climate for a specific geographical location is a crucial step to assess impacts of climate change on different sectors. This study included pool of 105 and 78 GCMs for representative concentration pathways (RCPs) 4.5 and 8.5, respectively, from Coupled Model Intercomparison Project—Phase 5, applied an advanced envelope-based selection approach to select representative GCMs for the Koshi river basin in China and Nepal at short-term (2016–2045), mid-century (2036–2065) and end-of-century (2071–2100) periods, and developed range of possible future precipitation and temperature scenarios with high resolution downscaled data ($10 \times 10 \text{ km}^2$), which is the novelty contribution of the study. Considering RCP4.5, average annual precipitation is expected to increase by 0–16%, 4–23% and 4–24% in the short-term, mid-century and end-of-century periods, respectively. Using RCP8.5, equivalent predictions are 6–20%, 6–36% and 13–49% in the short-term, mid-century and end-of-century periods, respectively. Average annual temperature is expected to increase, but with higher increases during winter than in the monsoon period. Considering RCP4.5, average annual temperature is expected to increase by 1–1.4°C, 1.3–1.9°C and 1.6–2.8°C in the short-term, mid-century and end-of-century periods, respectively. Similarly, using RCP8.5, equivalent predictions are 1–1.6°C, 1.8–2.9°C and 3.1–5.6°C in the short-term, mid-century and end-of-century periods, respectively. The ensemble mean of absolute change in average precipitation and temperature projects that High Himalaya and Tibet regions are more sensitive to climate change considering precipitation and temperature, respectively. The results also suggest that GCMs selection for a catchment varies with climate scenarios and specific future time periods.

KEYWORDS

climate change, end-of-century, GCM selection, Himalayan region, mid-century, RCPs

This is an open access article under the terms of the Creative Commons Attribution-NonCommercial-NoDerivs License, which permits use and distribution in any medium, provided the original work is properly cited, the use is non-commercial and no modifications or adaptations are made.

© 2019 The Authors. International Journal of Climatology published by John Wiley & Sons Ltd on behalf of the Royal Meteorological Society.

1 | INTRODUCTION

Climate change is a key driver of changes in the sustainability of Himalayan regions (Wester *et al.*, 2019). The Himalayan regions are very susceptible to global warming as vast areas over these regions are covered by snow and glaciers (Maskey *et al.*, 2011). Warming is more pronounced in these regions compared to lower elevation regions, and are particularly sensitive to global change and variability (Buytaert *et al.*, 2010; Shrestha and Aryal, 2011). The Himalayan regions are covered by snow throughout almost the whole year, and changes in precipitation and temperature pattern affect the snowmelt storage. The snowmelt rate is in turn linked to the hydrology of perennial Himalayan rivers. Changes in precipitation and temperature are expected to significantly affect the hydrology of the headwater basins in the Himalayan regions (Immerzeel *et al.*, 2009; Immerzeel *et al.*, 2012). As the likely impact of climate change in the Himalayan regions has a profound future implication on downstream water resources, it is of great concern to global communities (Eriksson *et al.*, 2009; Nepal *et al.*, 2014). Changes in the hydrological regime are expected due to changes in snowfall pattern and snowmelt resulting from climate change impacts (Nepal, 2016). Given this linkage, studies on climate change impacts on precipitation and temperature patterns in the Himalayan regions are essential.

General or global circulation models (GCMs), representing numerous atmospheric processes of the global climate system, are the main tools to estimate future climate patterns, and study likely changes in precipitation and temperature patterns. The number of GCMs available to predict future climate is both large and increasing. The number of GCM outputs applied in the Coupled Model Intercomparison Project (CMIP) Phase 3 (CMIP3) (Meehl *et al.*, 2007) and the CMIP Phase 5 (CMIP5) (Taylor *et al.*, 2012) are 25 and 61, respectively. The CMIP3 outcome archives were used for the Fourth Assessment Report (IPCC, 2007) while CMIP5 outcome archives were used for the Fifth Assessment Report (IPCC, 2013) of the Intergovernmental Panel on Climate Change (IPCC). Over this period of the time, there were large improvements in the way these models represent the present climate system and future projections.

Capacities of climate models/ensembles to represent climatic characteristics vary spatially and temporally. Many models/ensembles cannot perfectly simulate climatic characteristics and their capability to represent local climate varies spatially and temporally (Lee *et al.*, 2019). Gleckler *et al.* (2008) have reported that all climate models/ensembles are not equally skillful to represent the annual cycle climatology and the variance of monthly

anomalies. The complex topography of the Himalayan regions, and the coarse resolution of available GCMs has resulted in a weak consensus among models for these regions (Wester *et al.*, 2019). The selection of climate model(s) can vary depending on the objective of the model selection and future projections. In most cases, a single GCM is not sufficient to represent climatic characteristics of climatic extremes. These climatic extremes can be described as four corners of a quadrilateral representing cold and dry, cold and wet, warm and dry, and warm and wet conditions. For any chosen time and space, a specific climatic model/ensemble may demonstrate better abilities to represent climatic characteristics for a particular corner of a climatic extreme. Hence, the selection of global climate models with high capacities to represent the past and likely future climate for a specific geographical location is a crucial first step in assessing climate change impacts. Selecting GCMs from the large set of available climate models for a given location of interest is a challenging task.

The common approaches for the selection of GCMs are:

1. include all the models/ensembles with available data and simply take an average of all the predicted outcomes (Seager *et al.*, 2007), or
2. use a past performance approach focusing on the model's capacity to simulate past and present climate (Pierce *et al.*, 2009; Biemans *et al.*, 2013). In the past performance approach, hindcast data of model/ensemble are compared with observed data.

A major drawback of approach (a) is equal weighting given to the poor-performing and good-performing models (Pierce *et al.*, 2009). However, the past performance approach (hindcasting) may lead to an oversight of the possible futures (Lutz *et al.*, 2016), as hindcasting models which perform well (for the past climate periods) may not be able to represent future climate equally well. Another approach for the selection of climate models is the envelop approach, whereby GCMs are selected from a pool of available global models covering all possible future climate. In envelop approach, GCMs/ensembles are selected at each climatic extremes (four corners of a quadrilateral) based on annual means. Hence, four GCMs/ensembles are selected for a particular future study period to predict four possible future climatic scenarios. However, in approach (a), all the GCM runs are simply averaged and projection from only one dataset is used in contrast to four climatic corners in envelop approach. Hence, only one possible future is realized in approach (a). The main limitation of the envelope-based approach is that it only considers changes in annual means and

avoids the model's capacity to simulate climate process, as all the (global) model runs are considered to have equal plausibility (Lutz *et al.*, 2016).

Lutz *et al.* (2016) have recently developed a modified envelope-based approach for the selection of a representative global climate model, by combining the past-performance approach and the envelop approach. It focuses on simulating a workable number of climate model runs representing most likely future mean air temperature, annual precipitation and likely changes in climatic extremes. Such methods provide a range of possible future in terms of climate patterns. As there are still a large uncertainty in the future pathways to be adapted to control Green House Gaseous (GHG) emission, the future pathways are still uncertain. The uncertainty is mainly due to: (a) understanding of atmospheric processes which could be improved in the future, (b) socio-economic pathways adopted by the majority of the countries as a part of the UNFCCC Paris agreement, and (c) future technologies to control GHG emission. To address this uncertain future, we have used a three-step methodology in this research.

The spatial resolutions of GCMs are about 100–500 km in grid size with a temporal resolution of daily, monthly or a longer time step. Hence, they are not able to represent local scales, and the results should only be adopted at continental or global spatial scales for \geq monthly time periods (Trzaska and Schnarr, 2014). GCMs are unable to represent sub-grid scale features. For instance, local topography, land use and clouds as their outputs are at a relatively coarse spatial resolution, that is, approximately $250 \times 250 \text{ km}^2$ (Tisseuil *et al.*, 2010). Hydrological assessment of climate change impacts needs climate data at finer spatial scales, which limits direct use of GCM outputs at catchment level (Willems and Vrac, 2011). However, GCM outputs can be used to generate climate data at a finer scale to represent local climatic conditions. The process used to reduce the scale of any information finer than $100 \times 100 \text{ km}^2$ scales (spatially) and shorter than monthly values is called downscaling, and it assumes that the local climate is a combination of local conditions and large-scale atmospheric features (Trzaska and Schnarr, 2014).

Previous studies conducted on climate projections for the Koshi river basin are based on few GCMs and lack multiple criteria to select GCMs. Bharati *et al.* (2014) projected the precipitation and temperature on the Koshi river basin for 2030s and 2050s considering IPCC Special Report on Emission Scenarios (IPCC-SRES) A2 and B1 climate scenario. The study was performed by simply averaging the outputs of four GCMs. Agarwal *et al.* (2014) conducted study on Koshi river basin considering only 10 GCMs available in Long Ashton Research Station Weather Generator (LARS-WG) and projected

precipitation for 2011–2030, 2046–2065 and 2080–2099 considering the IPCC-SRES B1, A1B and A2 climate scenario. Likewise, Agarwal *et al.* (2016) projected the temperature patterns in the Koshi river basin considering the same climate scenario, study periods and GCMs as adapted by Agarwal *et al.* (2014). Nepal (2016) studied on the Koshi river basin considering IPCC-SRES A1B, and projected precipitation and temperature for 2040–2050 and 2086–2096. It considered Providing Regional Climates for Impact Studies (PRECIS) Regional Climate Model. Rajbhandari *et al.* (2017) also studied on the Koshi river basin, and projected precipitation and temperature parameters for 2011–2040 and 2041–2070 and 2071–2098 considering IPCC-SRES A1B. This study considered PRECIS Regional Climate Model. None of the above studies used CMIP5 GCM outputs and current RCPs. Furthermore, these studies did not apply any advance envelop approach on GCM selection and simply picked up GCM(s) from a pool of available GCMs.

Rajbhandari *et al.* (2016) projected precipitation and temperature patterns in the Koshi river basin for 2021–2050 considering (RCPs) 4.5 and 8.5. They selected one GCM for each corner from a pool of 43 GCMs for RCP4.5 and 41 GCMs for RCP8.5 based on the changes in the mean precipitation and temperature. Although Rajbhandari *et al.* (2016) have considered the current CMIP5 GCM outputs and RCP scenarios, the GCMs were selected based on the projected changes in the mean precipitation and temperature from a limited sets of GCM outputs, without considering projected changes in climatic extremes and past performance of GCMs to simulate annual cycle. Also, they did not downscale at high resolution and rely their outcomes on GCM cells which is about 250 km.

In this regard, we explore here the use of GCM outputs to estimate precipitation and temperature patterns with various global warming scenarios at short-term, mid-century and end-of-century time periods. Such analysis will be useful to understand the impact of climate change on the hydrological regime. The main purpose of this paper is to: (a) select representative GCMs, and (b) develop range of possible future climatic scenarios based on high-resolution downscaled climate data for the Koshi river basin located in China and Nepal. Initially, the methodology focuses on the selection of the representative GCMs for the study area. Then, it applies the selected models for the downscaling of precipitation and temperature at $10 \times 10 \text{ km}^2$ grids. Finally, based on downscaled data, future precipitation and temperature patterns of the Koshi river system for the three future time periods are presented.

This study includes pool of 105 and 78 GCMs; considers projected changes in climatic mean, climatic

extremes and past performance of GCMs to simulate annual cycle; and includes present climate scenarios (RCP4.5 and RCP8.5) to select representative GCMs for the study area, and develops range of possible future climatic scenarios with high-resolution downscaled data ($10 \times 10 \text{ km}^2$), which is the novelty contribution of the study. This study addresses the limitations of the previous studies and provides new climatological insights for the region.

2 | STUDY AREA AND DATA

The Koshi river, one of the largest tributaries of the Ganges, originates in China and flow through Nepal and India. The Koshi river basin is the largest river basin in Nepal, and about 22% of Nepal's population or 5.8 million people, live within this basin (Dixit *et al.*, 2009). The catchment area of the Koshi basin near Chatara in Nepal is about $54,006 \text{ km}^2$ ($28,080 \text{ km}^2$ in Tibet [China] and $25,926 \text{ km}^2$ in Nepal), delineated using ArcSWAT. The catchment areas in Nepal with High Himalaya (elevation $>3,000 \text{ m}$) and Lower Himalaya (elevation $<3,000 \text{ m}$) are $8,257$ and $17,669 \text{ km}^2$, respectively. The altitude in the Nepalese part of the catchment area varies from 97 m above mean sea level (a.m. s.l.) in the southern part, to 8848 m a.m.s.l. in the northern part of the High Himalayas. The altitude in Tibet part varies from $1,018$ to $>8,792 \text{ m}$. The location

of the catchment area of the Koshi river basin in China and Nepal is shown in Figure 1.

From the initial pool of climate models, this study used the ensemble of model runs for RCPs 4.5 and 8.5, which are available in the CMIP5 repository (Taylor *et al.*, 2012). The RCPs 4.5 and 8.5 are mentioned in Section 3.1 under the selection of representative pathways. The total number of model runs available for RCP4.5 is 105, whereas 78 model runs are available for RCP8.5. The RCP4.5 and RCP8.5 model runs were downloaded from the Royal Netherlands Meteorological Institute (KNMI) climate explorer (<https://climexp.knmi.nl/start.cgi>) in July 2018. The indices as per Expert Team on Climate Change Detection and Indices (ETCCDI) (Peterson, 2005) were calculated from the database constructed by Sillmann *et al.* (2013a, 2013b), and available in <https://climexp.knmi.nl/start.cgi> in July 2018. This database does not include all the model ensembles. For those model ensembles that are not included in the database, the GCMs were downloaded from climate4impact (<https://climate4impact.eu/impactportal/general/about.jsp>) in July 2018 then the ETCCDI indices were calculated using the Climate Data Operator (CDO-version 1.6.4), developed by Max-Planck Institute for Meteorology (<https://code.mpimet.mpg.de/projects/cdo/files>). The climate data operator (CDO) is a collection of more than 600 command line operators for standard processing of climate data (Max-Planck Institute for Meteorology, 2018). The relevant CDO command line

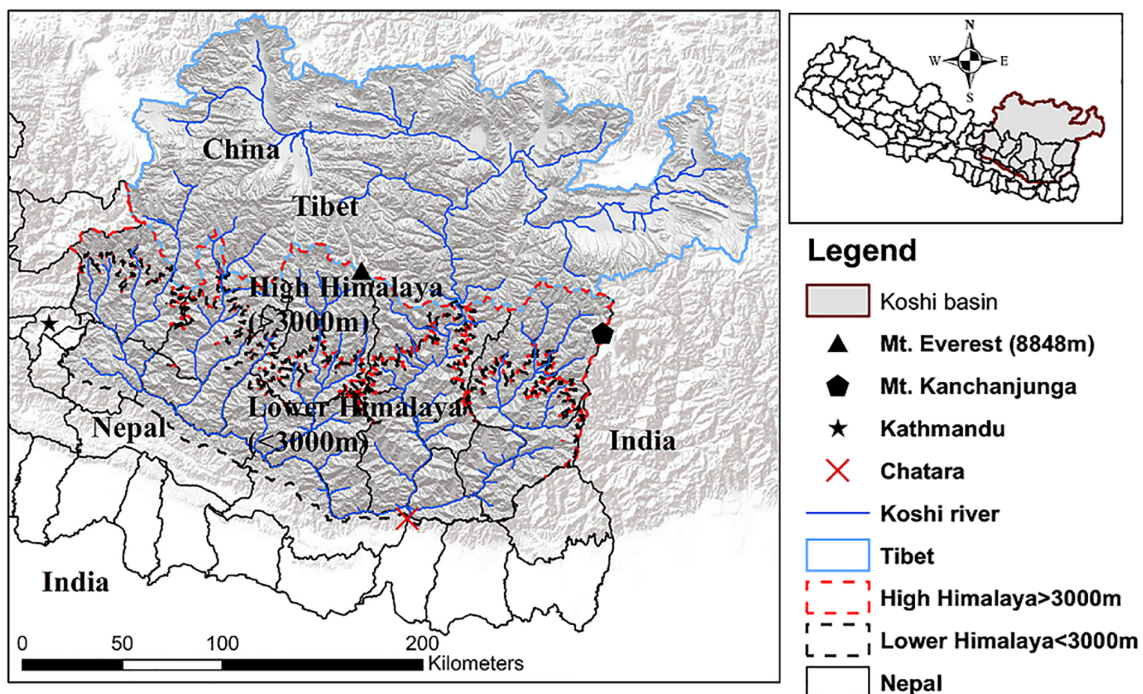


FIGURE 1 Study area, the Koshi river basin down to Chatara

operators were used through R programming (RStudio Team, 2016) applying the same procedures as Sillmann *et al.* (2013a), Sillmann *et al.* (2013b). To evaluate past-performance of individual GCM runs in simulating the annual cycle of air temperature and precipitation, the Hi-AWARE reference climate dataset developed by Lutz and Immerzeel (2015) was used. The datasets can be downloaded from <http://rds.icimod.org/clim>. The climate dataset for Indus, Ganges and Brahmaputra river basins were prepared by using Watch Forcing based on ERA-interim dataset, which was bias corrected by using Global Precipitation Climatology Centre (GPCC) and glacier mass balance data. Since ERA-interim and GPCC were also derived based on observed stations, it is assumed that they represent the regional climatic patterns. However, because of their regional nature, sub-variability is expected within the sub-set. For this assessment, additional bias correction using stations data is not carried out.

3 | METHODS

3.1 | Selection of representative concentration pathways

IPCC (2014) has documented four representative concentration pathways (RCPs) to predict possible global future climate scenarios in the fifth Assessment Report. The RCPs are based on the level of greenhouse gas concentration (CO_2 , CH_4 , N_2O , etc.) and represent the range of radiative forcing values by the year 2100. The RCPs and their corresponding radiative forcing along with a CO_2 -equivalent concentration in 2100 (IPCC, 2014), are represented in Figure 2 (adapted from Van Vuuren *et al.*, 2011a), and are summarized below:

- RCP2.6 (Green): Peak in radiative forcing at $\sim 3 \text{ W/m}^2$ (430–480 ppm CO_2 -eq) and then decline to 2.6 W/m^2 by 2100.

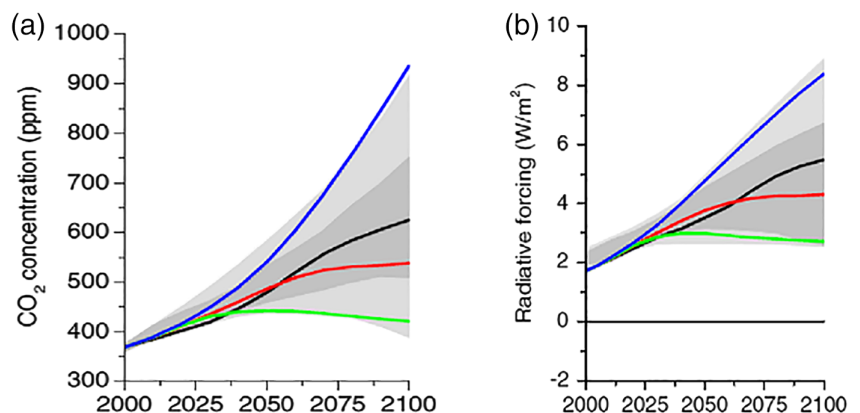
- RCP4.5 (Red): Stabilization without overshoot to 4.5 W/m^2 (580–720 ppm CO_2 -eq) and then stabilized after 2100.
- RCP6.0 (Black): Stabilization without overshoot to 6.0 W/m^2 (720–1,000 ppm CO_2 -eq) and then stabilized after 2100.
- RCP8.5 (Blue): Rising radiative forcing to 8.5 W/m^2 ($>1,000$ ppm CO_2 -eq) by 2100

The RCP2.6 represents the low end of the climate scenario in terms of emission and radiative forcing (Van Vuuren *et al.*, 2011b). This pathway has been shown to be technically feasible, but requires the immediate and wide participation of all the countries in the world in a large portfolio of mitigation options (Van Vuuren *et al.*, 2010). As a major decline of greenhouse gas emission in the short run seems unrealistic (Lutz *et al.*, 2016), it is unlikely that the RCP2.6 scenario can be accepted and is not considered further in this research. Among the remaining RCPs, one stabilization scenario, RCP4.5, and one high emission scenario, RCP8.5, are analysed in this research. Within the stabilization scenarios (RCP4.5 and RCP6.0); RCP4.5 is chosen as it represents the lower end of the stabilization scenarios. RCP4.5 and RCP8.5 should cover the entire range of stabilization and high emission scenarios, and hence were selected for this research.

3.2 | Selection of study periods

National Planning Commission, Nepal is an apex advisory body of the Government of Nepal for articulating national vision, development policies, periodic plans and sectoral policies for the development of the nation. Development policies and programs in Nepal are based on 5-year Periodic Plans prepared by the National Planning Commission. The findings of this research would be helpful for the National Planning Commission while preparing the development policies and programs in the climate

FIGURE 2 RCPs with (a) CO_2 concentration and (b) corresponding radiative forcing (adapted from Van Vuuren *et al.*, 2011a)



change context. Consequently, this study focuses on three study periods: short-term (2016–2045), mid-century (2036–2065), and end-of-century (2071–2100) periods each covering a 30-year time window. The GCMs selection is carried out for each time period which can result in different model selections for each time period.

3.3 | General circulation model selection approach and downscaling

An advanced envelope-based selection approach developed by Lutz *et al.* (2016) is applied to select the representative climate models for RCP4.5 and RCP8.5 for the short-term, mid-century and end-of-century periods. The flow diagram of the approach adopted is shown in Figure 3 (adapted from Lutz *et al.*, 2016). This approach included three main steps as described in the following sections:

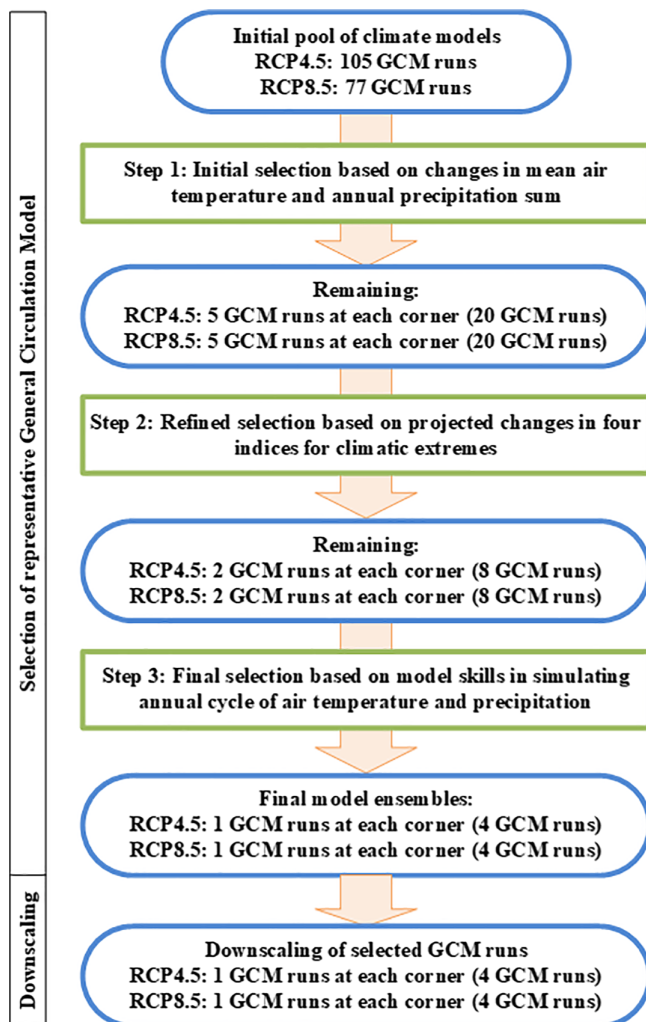


FIGURE 3 Flow chart for General Circulation Model selection and downscaling (adapted from Lutz *et al.*, 2016)

3.3.1 | Step 1: Initial model selection based on changes in climatic means (mean air temperature and annual precipitation)

First, area-averaged monthly mean air temperature and monthly total precipitation time series data for the RCP4.5 and RCP8.5 model runs were downloaded from <https://climexp.knmi.nl/start.cgi> as mentioned in Section 2. The KNMI datasets are available at a resolution of $2.5 \times 2.5^\circ$ (i.e., approximately $250 \times 250 \text{ km}^2$). The Koshi river basin, down to Chatara in Nepal, lies within latitude $26^\circ 50' - 29^\circ 08' \text{N}$ and longitude $85^\circ 23' - 88^\circ 56' \text{E}$. So, the boundary between 24° and 31°N and 84° and 91°E was selected in the KNMI dataset to cover the entire catchment of the study area. The models/ensemble having both the precipitation and temperature data, 105 GCMs for RCP4.5 and 78 GCMs for RCP8.5, were considered for initial selection. R programming (RStudio Team, 2016) was used to download and analyse the data.

Second, the mean air temperature and annual total precipitation for each year of the base period (1981–2010) and future periods (short-term, mid-century and end-of-century) were calculated. The ranges of predicted changes in annual mean air temperature and annual total precipitation for the reference and future periods were calculated for the study area. The delta changes for temperature ($^\circ \text{C}$), ΔT , and precipitation (%), ΔP , in these three study periods were also calculated. Based on the ΔT and ΔP values for all the model/ensemble, the 10th and 90th percentile values of ΔT and ΔP were determined for RCP4.5 and RCP8.5, considering short-term, mid-century, and end-of-century periods as per standard practice (Lutz *et al.*, 2016). The 10th and 90th percentile values of ΔT and ΔP represent the cold and warm sides of the temperature and dry and wet sides of precipitation extremes, respectively. The four corners (in Figure 4), cold and dry, warm and dry, cold and wet, and warm and wet, represent the four extreme climates, which are 10th and/or 90th percentile values of ΔT and ΔP . For example, the cold and dry corner represents the 10th percentile of ΔT and 10th percentile of ΔP . Likewise; the warm and wet corner represent the 90th percentile of ΔT and 90th percentile of ΔP .

The proximity of the model run's percentile rank scores to each corner with respect to their projections for ΔT and ΔP for the entire ensemble was calculated using Equation 1 viz:

$$D_{p_i^p, p_j^r} = \sqrt{(P_i^p - P_j^p)^2 + (P_i^r - P_j^r)^2} \quad (1)$$

and P_j^r , respectively) to the corner under consideration, which are 10th and/or 90th percentile score of both ΔP

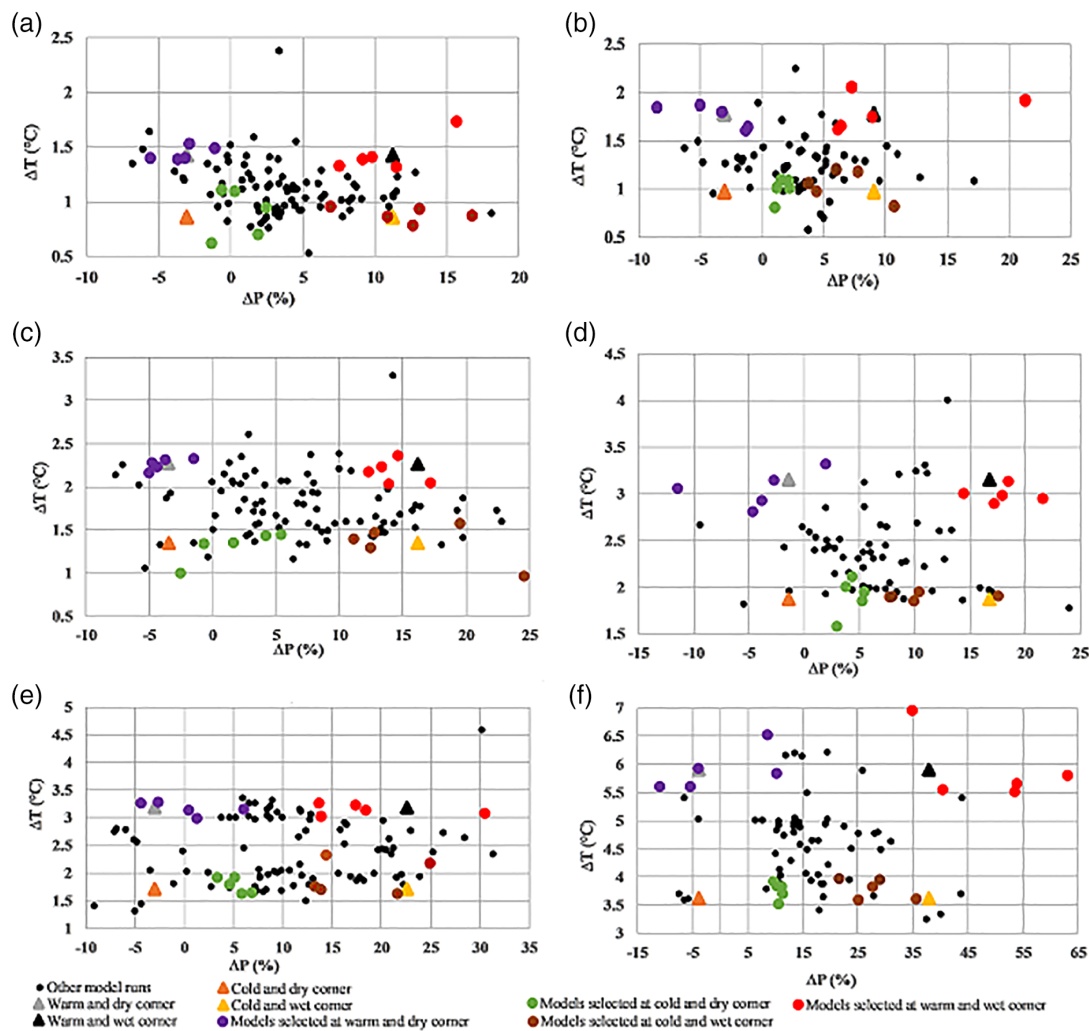


FIGURE 4 Projected changes in ΔT and ΔP between (a) 2016–2045, RCP4.5 (b) 2016–2045, RCP8.5 (c) 2036–2065, RCP4.5 (d) 2036–2065, RCP8.5 (e) 2071–2100, RCP4.5 (f) 2071–2100, RCP8.5 and the base period (1981–2010) for all the included GCM runs

and ΔT for the entire ensemble (P_j^P and P_j^T , respectively). P_j^P and P_j^T values are 10th and/or 90th percentile values of ΔP and ΔT for the entire ensemble for the particular corner. P_j^P and P_j^T are the percentile rank values of model j for ΔP and ΔT , respectively.

Finally, the GCMs/ensembles were then ranked based on their proximity to each corner. Experimental data availability at a temporal resolution of daily time step for each model was then checked, as daily data are required for empirical-statistical downscaling. In this study, daily data availability for parameters of interest (temperature and precipitation) was checked from <https://climate4impact.eu/impactportal/general/about.jsp> as mentioned in Section 2. Based on the ranking of the models, considering the proximity to the respective corner and daily data availability, five models at each corner were selected for the next step (Step 2—Figure 3).

3.3.2 | Step 2: Refined model selection based on projected changes in climatic extremes (four indices)

Five models at each corner for RCP4.5 and RCP8.5 selected separately from initial selection were further refined in the selection process based on projected changes in four indices for climatic extremes. These indices are described in Table 1. Two climatic extremes from both air temperature and precipitation were assessed considering the changes in indices based on the ETCCDI (Peterson, 2005). Warm spell duration index (WSDI) and cold spell duration index (CSDI) were evaluated for climatic extremes in air temperature. Likewise, consecutive dry days (CDD) and the precipitation due to very wet days (R95pTOT) were considered for climatic extremes in precipitation.

TABLE 1 Description of ETCCDI indices used for refined model selection

Meteorological variable	ETCCDI index	Index description
Air temperature	WSDI	Warm spell duration index: Count of days in a span of at least 6 days when $TX_{ij} > TX_{in90}$ where TX_{ij} is the daily maximum temperature on day i in a year j , and TX_{in90} is the 90th percentile of daily maximum temperature for the base period (1981–2010).
Air temperature	CSDI	Cold spell duration index: Count of days in a span of at least 6 days when $TN_{ij} < TN_{in10}$, where TN_{ij} is the daily minimum temperature on day i in a year j , and TN_{in10} is the 10th percentile of daily minimum temperature for the base period (1981–2010).
Precipitation	CDD	Consecutive dry days: Maximum length of dry spell when $P_{ij} < 1$ mm where P_{ij} is daily precipitation amount on day i in a year j .
Precipitation	R95pTOT	Precipitation due to very wet days: Annual total precipitation when $P_{ij} > P_{in95}$, where P_{ij} is the daily precipitation amount on a wet day (precipitation ≥ 1 mm) i in a year j , and P_{in95} is the 95th percentile of precipitation on wet days in the base period (1981–2010).

The results of the climate model ensembles will be used to assess the impacts on hydrological aspects, especially water availability for irrigation purposes, and the agricultural water management practices. In this regard, WSDI and CSDI are considered as they affect the snow and ice accumulation/melt process, which is an important factor in the upstream part of the Himalayan river basin, where the Koshi river basin is situated. These extreme temperature indices also affect the evapotranspiration and water requirement for crops. CDD is vital for both precipitation extreme and dry spells affecting the crop growth. The results of climate model ensembles in this research will be applied for irrigation and agricultural water management purposes, hence R95pTOT is used in this research.

For the refined selection purpose, the changes in WSDI, CSDI, CDD and R95pTOT were calculated as described in Section 2. After calculating all the indices values for initially selected model ensembles for each RCP4.5 and RCP8.5 for short-term, mid-century and end-of-century periods, relevant indices were selected for each corner. For example, CSDI and CDD represent the cold and dry corner. Likewise, WSDI and CDD for the warm and dry corner and CSDI and R95pTOT for the cold and wet corner. Similarly, WSDI and R95pTOT represent the warm and wet corner. Following Lutz *et al.* (2016), the model ensembles were scored (T_{index} rank and P_{index} rank) based on the percentage increase of relevant indices. The largest increase scored five point, whereas the smallest increase scored 1. The T_{index} and P_{index} were then averaged to calculate the combined score. The two model ensembles with highest combined score were selected for the next step (Step 3—Figure 3).

3.3.3 | Step 3: Final model selection based on past performance (model capability in simulating the annual cycle of air temperature and precipitation)

The model ensembles selected from the refined selection were then assessed for their capability to simulate the annual cycle of air temperature and precipitation for the base period (1981–2010). The Hi-AWARE reference climate dataset were downloaded from <http://rds.icimod.org/clim>. For air temperature, total bias, monsoon bias, and winter bias were considered. The biases represent the difference between the reference value and the GCMs/ensembles runs for the same period. Precipitation in the Koshi basin is highly influenced by the monsoon. Winter (dry) season precipitation is also crucial for irrigation demand of winter season crops. So, winter bias, monsoon bias and total bias (annual) were used to calculate biases for precipitation and temperature between the reference data and the GCM ensemble data. The biases for precipitation and temperature were calculated in percentage and °C, respectively. The precipitation bias (P_{bias}) and temperature bias (T_{bias}) values were used to evaluate the GCM/ensemble's capability in simulating the annual cycle of air temperature and precipitation.

The bias values (P_{bias} and T_{bias}) were then normalized (each absolute bias value expressed as a fraction of the largest absolute bias value) within the model ensembles for each scenario, RCP4.5 and RCP8.5. P_{bias} score and T_{bias} score were calculated by averaging the precipitation biases and temperature biases, respectively. Then, the sum of P_{bias} score and T_{bias} score was calculated to find the combined score. The model ensemble with the least combined score, representing the least

variation in reference values and GCM runs for the base period, was selected at each corner.

Based on the selected model ensembles for different corners, the climate data downscaling was conducted as described in the following section.

3.3.4 | Climate data downscaling for the Koshi basin

Downscaling methods

Downscaling techniques are basically classified into two types: statistical and dynamical. Statistical downscaling techniques develop a statistical relationship between local climate variables and large-scale GCM outputs, whereas dynamical downscaling techniques use high-resolution Regional Climate Models (RCMs) nested within a GCM to generate local weather variables (Chen *et al.*, 2010). The dynamical approach may better represent meso-scale disturbances that play crucial roles in the regional scale, which cannot be represented in low-resolution GCMs (Lee *et al.*, 2014). As spatial resolution of RCMs is higher, they describe more realistic topographic characteristic (Lee and Hong, 2014). Although RCMs are successfully applied in dynamical downscaling, the regional predictability and the evaluation of added values to the GCM outputs have still not been clarified, and the error sources in regional downscaling are still vague (Hong and Kanamitsu, 2014). Dynamical downscaling requires huge data sets which makes it computationally intensive and time-consuming and is only recommended for projects having research periods of more than 2 years (Trzaska and Schnarr, 2014). In contrast, statistical downscaling are easier methods to apply and interpret, while their spatial resolution is also finer than that of RCM (Trzaska and Schnarr, 2014). The complex physical processes may not be fully represented in statistical downscaling and the downscaled variables might not guarantee physical consistency between them (Lim *et al.*, 2007). However, statistical downscaling has advantages over dynamical downscaling in that important characteristics of regional climates are analysed in training period and then they are included in the subsequent downscaling process (Lim *et al.*, 2007). Moreover, statistical downscaling is less resource intensive too. The common approaches for bias correction in statistical downscaling are delta change, multiple linear regression, analogue, local intensity scaling, and quantile mapping. Themeßl *et al.* (2011) compared the performance of seven empirical-statistical downscaling and error correction methods (multiple linear regression, multiple linear regression with cube root transformation, multiple linear regression with randomization, analogue, nearest neighbour analogue, local

intensity scaling, and quantile mapping) and concluded that quantile mapping outperforms all other methods.

Quantile mapping for climate data downscaling

The spatial resolution of the reference dataset is $10 \times 10 \text{ km}^2$. The spatial resolution of selected GCMs ($\sim 250 \text{ km}$) was made finer ($10 \times 10 \text{ km}^2$) applying bilinear interpolation in R programming to match it with the spatial resolution of reference dataset. Then, quantile mapping was applied for bias correction at a finer resolution of $10 \times 10 \text{ km}^2$. The main steps involved in the downscaling are (a) converting coarse GCM resolution ($\sim 250 \text{ km}$) into 10 km finer resolution, (b) creating empirical cumulative distribution function for each month based on daily data between GCM and reference grid, and finally (c) applying correction function on a daily basis for each finer resolution grid cell. In this way, both the bias correction and downscaling is conducted applying the quantile mapping.

Quantile mapping (QM) uses empirical cumulative density functions (ecdf). The ecdf of a parameter is a non-parametric estimator of the underlying cumulative distribution function. Basically, ecdf sorts all the data (n , number of data) in ascending order and assigns a probability of $1/n$ to each data. QM originated from the empirical transformation of Panofsky and Brier (1968) and has been successfully applied in the hydrological application (Boé *et al.*, 2007; Themeßl *et al.*, 2011). QM compares the ecdf of a climate variable in historical observation with that of the GCMs outputs and defines a correction function depending upon the quantile. The quantile is used to correct the variable data sets of GCM outputs based on the respective quantile (Boé *et al.*, 2007; Themeßl *et al.*, 2011; Themeßl *et al.*, 2012). As described by Themeßl *et al.* (2012), it is applied on a daily basis (t) for each grid cell (i) separately resulting in a corrected time series $Y_{t,i}^{\text{cor}}$ (Equation 2) using correction function $CF_{t,i}$ (Equation 3) viz:

$$Y_{t,i}^{\text{cor}} = X_{t,i}^{\text{GCM}} + CF_{t,i} \quad (2)$$

$$CF_{t,i} = \text{ecdf}_{\text{month},i}^{\text{obs,ref}^{-1}}(P_{t,i}) - \text{ecdf}_{\text{month},i}^{\text{GCM,ref}^{-1}}(P_{t,i}) \quad (3)$$

$$P_{t,i} = \text{ecdf}_{\text{month},i}^{\text{GCM,ref}}(X_{t,i}^{\text{GCM}}) \quad (4)$$

where, $Y_{t,i}^{\text{cor}}$ is a corrected time series on a daily basis (t) within the study period for each grid cell (i) over the study area, $X_{t,i}^{\text{GCM}}$ is the GCM time series on a daily basis (t) within the study period for each grid cell (i) over the study area: $CF_{t,i}$ is correction function on a daily basis (t) within the study period for each grid cell (i) over the study area. Likewise, $\text{ecdf}_{\text{month},i}^{\text{obs,ref}^{-1}}(P_{t,i})$ is the observed

inverse ecdf (ecdf^{-1}) for the particular day of the year in the reference period at probability P ($P_{t,i}$): $\text{ecdf}_{\text{month},i}^{\text{GCM,ref}^{-1}}(P_{t,i})$ is the GCM inverse ecdf (ecdf^{-1}) for the particular day of the year in the reference period at probability P ($P_{t,i}$), and $\text{ecdf}_{\text{month},i}^{\text{GCM,ref}}(X_{t,i}^{\text{GCM}})$ is the GCM ecdf for the particular day of the year in the reference period for each grid cell (i) over the study area.

The correction function represents the difference between observed (obs) and the GCM inverse ecdf (ecdf^{-1}) for the particular day of the year in the reference period at probability P ($P_{t,i}$). P is obtained by relating the GCM data (X^{GCM}) to the corresponding ecdf in the reference period. This results in corrected time series Y^{cor} to create the bias-corrected dataset.

This basic QM procedure may result in a methodological problem when the dry-day frequency in the GCM data ($\text{ecdf}^{\text{GCM,ref}}$) is greater than in the observations ($\text{ecdf}^{\text{obs,ref}}$) (Themeßl *et al.*, 2012). This results in a systematic wet precipitation bias, as any dry day in X^{GCM} is mapped to a precipitation day in observed dataset. Consequently, frequency adaptation (FA) is applied to extend the basic QM procedure. In order to account for a methodological problem (Themeßl *et al.*, 2012). With FA, only the fraction (ΔP_0) (Equation 5) of such dry-day cases with probability P_0 are corrected randomly by linearly interpolating between zero precipitation and the precipitation amount of $\text{ecdf}_{\text{month},i}^{\text{obs,ref}^{-1}}(\text{ecdf}_{\text{month},i}^{\text{GCM,ref}}(0))$ (the first precipitation class in QM without FA). It will reduce the wet bias in the GCM dataset as:

$$\Delta P_0 = \frac{\text{ecdf}_{\text{month},i}^{\text{GCM,ref}}(0) - \text{ecdf}_{\text{month},i}^{\text{obs,ref}}(0)}{\text{ecdf}_{\text{month},i}^{\text{GCM,ref}}(0)} \quad (5)$$

In climate change impact studies, precipitation and temperature values in future may exceed the greatest value found in the reference period. For values of extremes that are outside the range of the reference period, corrections are made by including constant linear extrapolation of the correction value that is, the difference between $\text{ecdf}^{\text{obs,ref}}$ and $\text{ecdf}^{\text{GCM,ref}}$ at the highest and lowest quantiles (Boé *et al.*, 2007; Themeßl *et al.*, 2012). In such case, the future corrected value is calculated by applying Equation 6 viz:

$$P_{\text{fut,cor}} = \max(P_{\text{obs}}) * \frac{P_{\text{fut,GCM}}}{\max(P_{\text{fut,GCM}})} \quad (6)$$

4 | APPLICATION OF METHODOLOGY, RESULTS AND DISCUSSIONS

The application of the methodology described above is demonstrated in the following sections.

4.1 | General circulation model selection

4.1.1 | Selection of 5 GCM runs at each corner based on changes in mean air temperature and annual precipitation (step 1)

The projected changes in mean air temperature (ΔT) and annual precipitation (ΔP) between future study periods (short-term, mid-century and end-of-century) and base period are the basis for the initial model selection for corresponding future study periods (Figure 4). The ΔT and ΔP projections for mid-century are higher than for short-term, while the projections for the end-of-century period are much higher than the short-term and mid-century projections. Similarly, these projections for RCP8.5 model pool are much higher, particularly at the end-of-century period. The ΔT and ΔP range from 0.5 to 2.4°C and -6.9 to +18.1%, respectively, considering short-term period for RCP4.5 (Figure 4a), whereas for RCP8.5, these ranges are 0.6–2.2°C and -8.5 to +21.3% (Figure 4b). The ΔT and ΔP ranges are 1–3.3°C and -7.6 to +3.3%, respectively, considering mid-century period for RCP4.5 (Figure 4c), whereas for RCP8.5, these ranges are 1.6–4.0°C and -11.5 to +24.0% (Figure 4d). Likewise, the ΔT and ΔP ranges are 1.3–4.6°C and -9.1 to +31.4%, respectively, considering end-of-century period for RCP4.5 (Figure 4e), whereas for RCP8.5, these ranges are 3.3–7.0°C and -11.0 to +63.0% (Figure 4f). The proximity of each GCM runs to each corner is calculated by applying Equation 1 as described in Section 3.3.1. The five models that are closest to each corner, and that have daily data available, are selected for Step 2. They are highlighted with colours in Figure 4. The proximity of selected model ensembles to respective corners differ substantially, as many of the model outputs are not available at daily time steps.

The models selected for various corners under different study periods are listed in Tables S1–S3.

4.1.2 | Selection of 2 GCM runs at each corner (Step 2)

For the models selected from the initial selection (Step 1), the projected changes in four ETCCDI indices between the short-term, mid-century and end-of-century periods; and the base period are calculated. The two model ensembles, for each corner, with the highest combined score were selected for next step (Step 3). In some corners, more than two model ensembles were selected as they have same second highest combined scores. Selected models, from Step 2, for short-term, mid-century and

end-of-century periods, are highlighted with blue colour in Tables S1–S3, respectively. In general, models projecting large changes in means (ΔT and ΔP) also project large changes in extreme indices. The model Can-ESM2_r2i1p1 (Table S1, for RCP4.5) projected the largest changes in ΔT (1.7°C) and ΔP (15.6%) in the warm and wet corner for short-term period, which also projected the largest increase in WSDI (194.4%) and R95pTOT (42.9%). This method of computing a combined score can result in the situation whereby models with the highest change in one ETCCDI indices are not selected due to the lowest change in another ETCCDI indices. For example, in the warm and dry corner, for the short-term period and RCP8.5, the model MPI-ESM-LR_r3i1p1 projects the largest changes in WSDI, however, it is not selected due to lower combined score compared to IPSL-CM5A-LR_r2i1p1 and MPI-ESM-LR_r1i1p1.

In Tables S1–S3, the models which are highlighted in blue will be used for the next step. The green and red highlighted values represent the percentage decrease and increase of the respective indices, respectively, during the analysis period.

All the models selected from the previous step show that CSDI is expected to decrease by 33–84% in short-term, 36–97% in mid-century and 47–99% in the end-of-century period considering RCP4.5. Likewise, CSDI is also expected to decrease by 35–93% in short-term, 58–99% in mid-century and 92–100% in end-of-century period considering RCP8.5. This predicts that warmer nights are expected in the future. The WSDI is expected to increase for all the study periods, 41–301% in short-term, 98–1,241% in mid-century and 60–2,601% in end-of-century period considering both the RCP4.5 and RCP8.5. Increase in WSDI predicts an increase in maximum temperature in future compared to the base period. Most of the model ensembles show that the CDD are expected to increase up to 19% in short-term, 34% in mid-century and 39% in end-of-century period considering both the RCP4.5 and RCP8.5. Similarly, most of the model ensembles show that the R95pTOT is expected to increase up to 58% in short-term, 79% in mid-century and 204% in end-of-century period considering both the RCP4.5 and RCP8.5. Increase in both the CDD and R95pTOT predicts more intense precipitation during the monsoon in the coming decades.

4.1.3 | Selection of 1 GCM run at each corner (Step 3)

The models were selected based on the lowest combined bias score (sum of precipitation bias score and temperature bias score) as shown in Tables S4. This method of

calculating a combined bias score can lead to the situation where models with the least P_bias score are not selected due to high T_bias score. For example, in the cold and dry corner, RCP4.5, in Table S4, the model inmcm4_r1i1p1 is not selected although it has least P_bias score (0.32), as it has high T_bias score (1.0) which results in combined bias score of 1.32. In contrast, its counterpart model, ACCESS1-3_r1i1p1, has a combined bias score of 0.75, with P_bias score and T_bias score as 0.54 and 0.2, respectively. The model ACCESS1-3_r1i1p1 was selected as it has the least combined score in the cold and dry corner.

Finally, selected models for different time periods and climatic extreme corners are highlighted in blue in Table S4. It shows that GCM selection for a catchment varies with future scenarios (RCP4.5 and RCP8.5) as well as future analysis periods (short-term, mid-century and end-of-century).

Most of the GCM ensembles share identical model code, for example, r1i1p1. Many CMIP5 experiments, that is, ensemble calculations were conducted using several realizations, r (also called initial states), initialization methods, i , and physics details, p . CMIP5 ensemble members are named in the r, i, p nomenclature followed by an integer. The majority of GCMs selected for the Koshi river basin for the short-term period for both RCPs are from ensemble member r1i1p1. For the mid-century, 3 of 4 GCMs share identical ensemble member r2i1p1 for RCP4.5, while for RCP8.5 all the GCMs share ensemble member r1i1p1. Likewise, majority of ensemble members are from r2i1p1 for RCP4.5 and from r1i1p1 for RCP8.5 for end-of-century period. Considering all three study periods, majority of ensemble members are from r2i1p1 for RCP4.5 and from r1i1p1 for RCP8.5.

The selected model outputs were used for downscaling the precipitation and temperature data and is described in the following sections.

4.2 | Climate data downscaling

Using the method described in Section 3.3.4, daily precipitation and average temperature GCM data are downscaled for each grid (grid size = $10 \times 10 \text{ km}^2$) for the entire Koshi river basin down to Chatara in Nepal (see Figure 1). GCM data were downscaled for each selected GCMs at different time periods and climatic extreme corners. For example purposes, the daily precipitation and temperature data for the years 2010, 2045, 2065 and 2100 (ending year of the base period, short-term, mid-century and end-of-century periods) for the selected model Can-ESM2_r3i1p1, which represents the warm and wet corner for RCP8.5 and end-of-century period, are shown in Figures S1 and S2.

4.2.1 | Precipitation

The absolute and percentage changes in average annual, winter, pre-monsoon, monsoon and post-monsoon precipitation in short-term, mid-century and end-of-century periods compared to the reference precipitation datasets are shown in Table 2. The winter, pre-monsoon, monsoon and post-monsoon seasons refer to December–February, March–May, June–September and October–November, respectively.

Average annual precipitation is expected to increase in the future: 0–16% in short-term, 4–23% in mid-century and 4–24% in end-of-century period, considering the RCP4.5 scenario. Higher precipitation is expected in scenario RCP8.5 compared to RCP4.5 scenario because average annual precipitation is expected to increase by 6–20% in short-term, 6–36% in mid-century and 13–49% in end-of-century period. Winter precipitation is expected to decrease for all the scenarios and study periods, except for the end-of-century period with RCP8.5. The pre-monsoon precipitation is also expected to decrease in coming decades. Monsoon precipitation is expected to increase in all scenarios and study periods. Similarly, post-monsoon precipitation is also expected to increase in future. Decreased winter and pre-monsoon precipitation and increased monsoon and post-monsoon precipitation with overall increased annual precipitation predict that more dry winter and wetter monsoon are expected in the future.

Table 2 shows large uncertainty in terms of future precipitation. For the short-term period, three of the four GCMs have predicted decrease in precipitation during winter (–53 to –9%) and however, one GCM has predicted an increase in precipitation by 21% for RCP4.5 scenario. In contrast, only one GCM out of four GCMs has predicted decrease in monsoon precipitation (–5%) while remaining three GCMs have predicted increase in precipitation (13–18%). For the mid-century period, three of the four GCMs have predicted decrease in precipitation during winter (–32 to –9%) and pre-monsoon (–39 to –9%), however, one GCM has predicted an increase by 13 and 15%, respectively, for RCP4.5 scenario. In contrast, only one GCM out of four GCMs has predicted decrease in precipitation during monsoon (–1%) and remaining GCMs have predicted an increase by 13 to 27%. For the RCP8.5 scenario, three out of four GCMs have predicted decrease in precipitation during winter (–55 to –1%) and pre-monsoon (–42 to –2%), however, one GCM has predicted an increase by 6 and 4% during winter and pre-monsoon, respectively. For the end-of-century period, all the selected GCMs have predicted decrease in precipitation in winter and pre-monsoon for RCP4.5 scenario. For RCP8.5 scenario, three out of four GCMs have predicted decrease (–54 to –8%) in precipitation during pre-monsoon, however, one GCM has

TABLE 2 Uncertainty in absolute and percentages changes in average precipitation in the Koshi river basin compared to base period

Annual/seasonal precipitation	Short-term			Mid-century			End-of-century					
	RCP4.5			RCP4.5			RCP8.5					
	Absolute (mm)	Relative (%)	Absolute (mm)	Relative (%)	Absolute (mm)	Relative (%)	Absolute (mm)	Relative (%)	Absolute (mm)			
Annual	4 to 288	0 to 16	103 to 365	6 to 20	70 to 417	4 to 23	107 to 663	6 to 36	79 to 441	4 to 24	242 to 890	13 to 49
Winter	–30 to 12	–53 to 21	–24 to –6	–42 to –10	–18 to 8	–32 to 13	–32 to 4	–55 to 6	–14 to –1	–24 to –2	5 to 10	9 to 18
Pre-monsoon	–71 to –4	–26 to –1	–89 to –23	–32 to –8	–109 to 42	–39 to 15	–116 to 10	–42 to 4	–156 to –8	–56 to –3	–149 to 36	–54 to 12
Monsoon	–70 to 257	–5 to 18	83 to 331	6 to 24	–8 to 381	–1 to 27	159 to 574	12 to 41	34 to 448	3 to 32	282 to 788	21 to 56
Post-monsoon	42 to 132	48 to 152	28 to 147	32 to 169	28 to 163	33 to 187	36 to 237	41 to 272	27 to 151	31 to 173	77 to 217	88 to 249
Regional annual precipitation												
Tibet	–9 to 180	–0.5 to 10	71 to 168	4 to 9	86 to 367	5 to 21	122 to 366	7 to 21	167 to 431	7 to 24	253 to 766	14 to 43
High Himalaya	–31 to 312	–1 to 12	107 to 450	4 to 18	37 to 534	1 to 21	110 to 852	4 to 33	57 to 485	2 to 19	290 to 1,189	11 to 46
Lower Himalaya	–1.5 to 504	–0.7 to 25	71 to 625	4 to 31	42 to 476	2 to 24	54 to 1,077	3 to 54	–35 to 447	–2 to 22	198 to 992	10 to 50

predicted an increase by 12%. The uncertainty in post-monsoon period is large in all three study periods for both RCP4.5 and RCP8.5 scenarios. Although the percentage increase in precipitation in post-monsoon is high compared to monsoon season, the absolute increase in post-monsoon season is less compared to monsoon season. The rainfall quantity in post-monsoon season is less in the reference period and a small increase in precipitation amount in post-monsoon season results in higher percentage increase compared to monsoon season.

The precipitation pattern in the Tibet region, High Himalaya in Nepal with elevation >3,000 m, and Lower Himalaya in Nepal with elevation <3,000 m (see Figure 1) was also analysed and is summarized in Table 2.

Table 2 also shows that higher uncertainty in precipitation, -0.7 to 25% considering RCP4.5 and 4–31% considering RCP8.5, is expected in the Lower Himalaya region during short-term period. Likewise, higher uncertainty in precipitation is expected in the Lower Himalaya region during mid-century term, 2–24 and 3–54% considering RCP4.5 and RCP8.5, respectively. Similarly, higher uncertainty in precipitation is predicted in the Lower Himalaya regions during end-of-century period, -2 to 22% and 10–50% considering RCP4.5 and RCP8.5, respectively. The ensemble mean (average of 4 GCMs) of absolute and percentage changes in average precipitation compared to base period in the Koshi river basin is shown in Table 3. Table 3 shows that higher increase in precipitation is expected in High Himalaya region compared to Tibet and Lower Himalaya regions.

The ensemble mean of monthly precipitation for end-of-century period is shown in Figure 5. The ensemble mean for the reference period for both RCP4.5 and RCP8.5 is close to reference data, which shows that the skill of downscaling for the reference period is satisfactory. The spatial pattern of absolute change in ensemble mean precipitation compared to reference data during end-of-century period is shown in Figure 6. Figure 6a,b shows the ensemble mean of absolute change in precipitation during end-of-century considering RCP4.5 and RCP8.5 scenarios, respectively. Higher increase in precipitation is expected in High Himalaya region compared to Tibet and Lower Himalaya at the end-of-century period.

Present and future average annual precipitation values along with their standard deviation for four GCMs selected for RCP4.5 and RCP8.5 considering end-of-century period is shown in Figure 7a. In Figure 7, the blue and red lines represent the corresponding average values, Figure 7a precipitation and Figure 7b temperature, of four GCMs selected for RCP4.5 and RCP8.5, respectively. The black line represents the average values of the reference data. The sky blue and pink areas represent the standard deviation for four GCMs selected for

TABLE 3 Ensemble mean (4 GCMs) of absolute and percentages changes in average precipitation in the Koshi river basin compared to base period

Annual/seasonal precipitation	Short-term			Mid-century			End-of-century							
	RCP4.5			RCP8.5			RCP4.5			RCP8.5				
	Absolute (mm)	Relative (%)	Relative (%)	Absolute (mm)	Relative (%)	Relative (%)	Absolute (mm)	Relative (%)	Relative (%)	Absolute (mm)	Relative (%)	Relative (%)		
Annual	178	10	11	237	13	13	335	18	18	297	16	16	701	39
Winter	-8	-14	-25	-7	-12	-12	-8	-14	-14	-5	-9	-9	7	13
Pre-monsoon	-44	-16	-16	-34	-12	-12	-55	-20	-20	-54	-19	-19	-64	-23
Monsoon	142	10	13	206	15	15	294	21	21	276	20	20	619	44
Post-monsoon	88	101	79	71	82	82	105	120	120	80	92	92	139	160
Regional annual precipitation														
Tibet	114	6	7	206	12	12	249	14	14	223	13	13	631	36
High Himalaya	199	8	9	291	11	11	419	16	16	391	16	16	922	36
Lower Himalaya	231	12	14	252	13	13	431	22	22	226	11	11	770	39

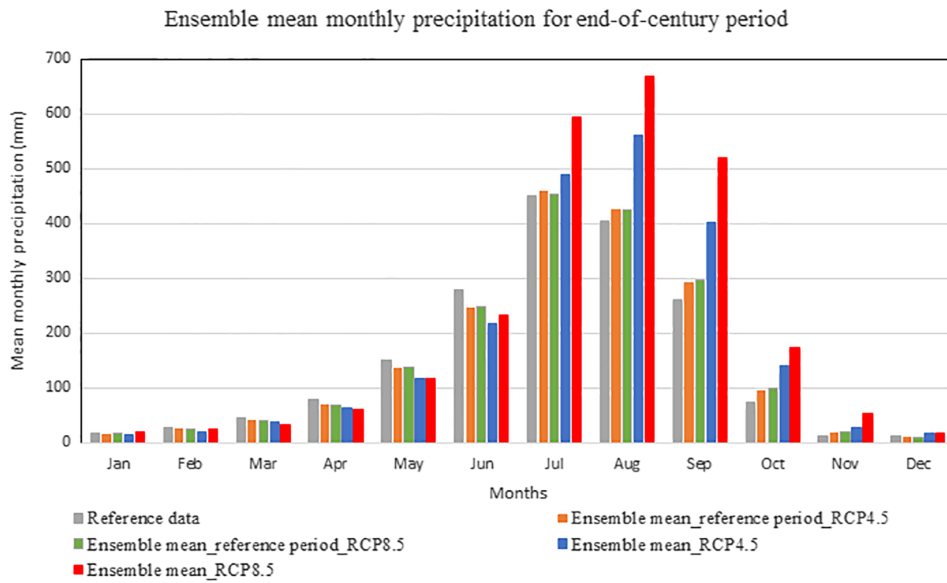


FIGURE 5 Ensemble mean monthly precipitation for end-of-century period

RCP4.5 and RCP8.5, respectively. The average annual precipitation in base period is 1,817 mm. The average annual precipitation values in short-term, mid-century and end-of-century periods are 2,011, 2,060 and 2,114 mm, respectively, for RCP4.5 scenario and 2018, 2098 and 2,518 mm, respectively for RCP8.5 scenario.

4.2.2 | Temperature

The uncertainty in average increase in annual, winter and monsoon temperature in short-term, mid-century

and end-of-century period as compared to the reference average temperature datasets is shown in Table 4.

The results show that there is a strong seasonal variability for temperature changes in the Koshi river basin. Average annual temperature is expected to increase in future (1–1.4°C in short-term, 1.3–1.9°C in mid-century and 1.6–2.8°C in end-of-century periods, considering RCP4.5 scenario). The higher increase in temperature is expected in scenario RCP8.5 as compared to RCP4.5 scenario. The average annual temperature is expected to increase in future by 1–1.6°C in short-term, 1.8–2.9°C in mid-century and 3.1–5.6°C in end-of-century period,

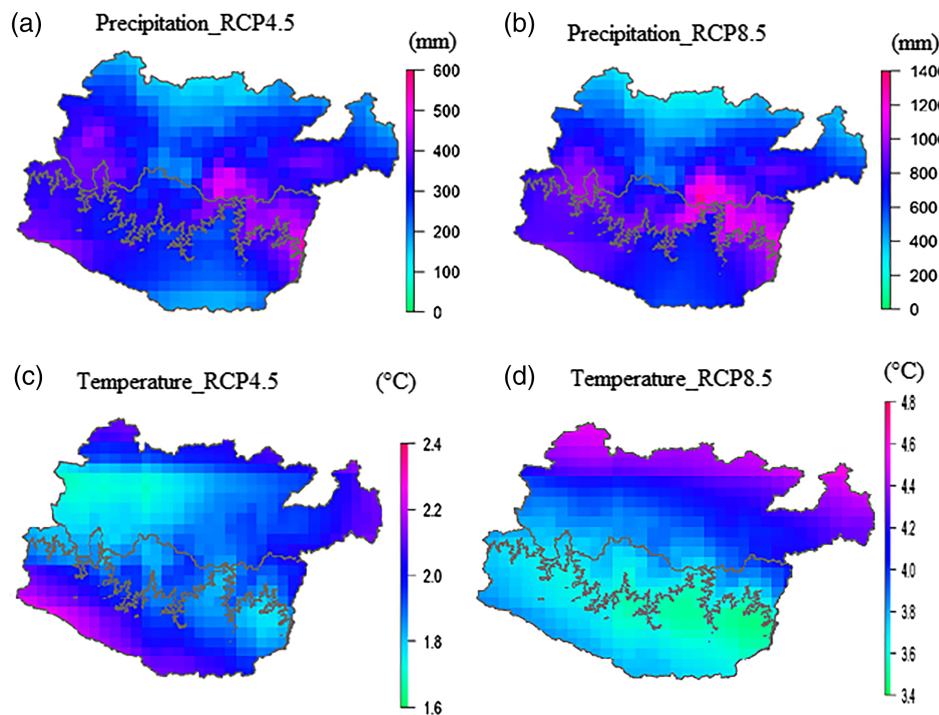
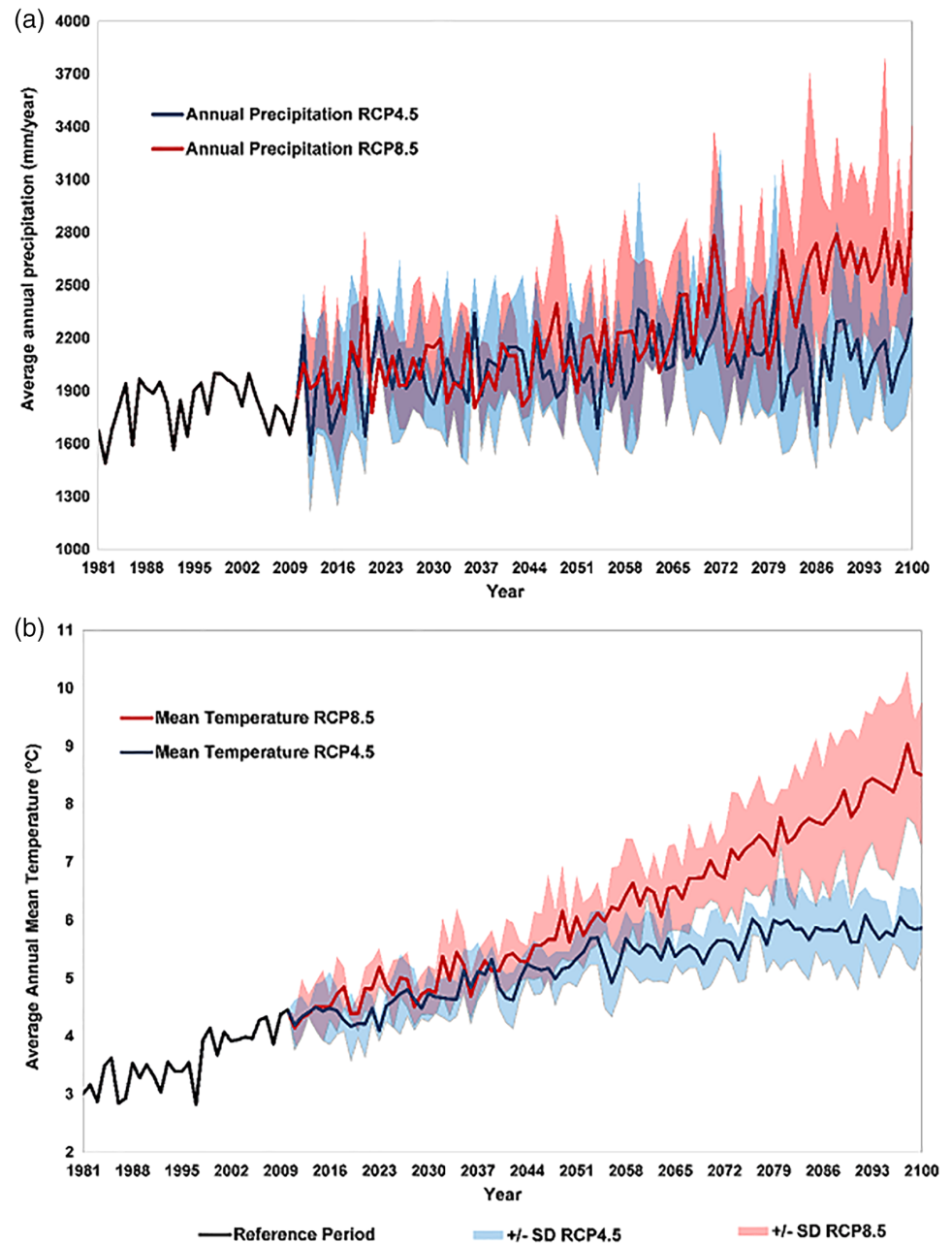


FIGURE 6 Ensemble mean of absolute change in average precipitation and temperature during end-of century period compared to reference period

FIGURE 7 Present and future average annual precipitation and temperature along with their standard deviation for the Koshi river basin



considering RCP8.5 scenario. The increment in winter temperature varies from 0.9–1.7, 1.3–2.1 and 1.7–2.9°C for short-term, mid-century and end-of-century periods considering RCP4.5 scenario. However, such increment in monsoon temperature varies from 0.7–1.3, 1.3–1.9 and 1.4–2.8°C for short-term, mid-century and end-of-century periods considering RCP4.5 scenario. Table 4 shows large uncertainty in terms of future mean temperature. Uncertainty in annual mean temperature is higher in RCP8.5 scenario compared to RCP4.5 scenario in all study periods. The results show that the uncertainty increases with future time period. For example, predicted increase in annual mean temperature in short-term, mid-century and end-of-century periods varies between 1.0 and 1.4°C,

1.3 and 1.9°C, and 1.6 and 2.8°C for RCP4.5 and 1.0–1.6, 1.8–2.9, and 3.1–5.6°C for RCP8.5, respectively. All the GCMs have predicted increase in annual mean temperature in future. Uncertainty in winter mean temperature is large compared to monsoon mean temperature.

The ensemble mean (average of 4 GCMs) of absolute and percentage changes in average temperature compared to base period in the Koshi river basin is shown in Table 5. Table 5 shows that higher increase in temperature is expected in Tibet region compared to High Himalaya and Lower Himalaya regions. Winter temperature is expected to increase more compared to that in the monsoon period for all study periods. The temperature pattern in the Tibet region, High Himalaya in Nepal, and Lower Himalaya in

TABLE 4 Uncertainty in absolute changes in average temperature in the Koshi river basin compared to base period

Annual/seasonal mean temperature	Short-term (°C increase)		Mid-century (°C increase)		End-of-century (°C increase)	
	RCP4.5	RCP8.5	RCP4.5	RCP8.5	RCP4.5	RCP8.5
Annual	1.0–1.4	1.0–1.6	1.3–1.9	1.8–2.9	1.6–2.8	3.1–5.6
Winter	0.9–1.7	1.1–1.6	1.3–2.1	1.8–3.9	1.7–2.9	2.9–7.8
Monsoon	0.7–1.3	0.8–1.4	1.3–1.9	1.8–2.9	1.4–2.8	3.0–4.4
Regional mean annual temperature						
Tibet	0.7–1.4	0.8–1.8	0.9–1.9	1.7–2.8	1.2–2.5	3.2–5.6
High Himalaya	0.7–1.1	0.8–1.3	1–1.5	1.4–2.5	1.3–2.5	2.7–5.1
Lower Himalaya	0.6–1.0	0.8–1.4	1.2–1.4	1.4–2.4	1.5–2.6	2.5–5.0

TABLE 5 Ensemble mean (4 GCMs) of absolute changes in average temperature in the Koshi river basin compared to base period

Annual/seasonal mean temperature	Short-term (°C increase)		Mid-century (°C increase)		End-of-century (°C increase)	
	RCP4.5	RCP8.5	RCP4.5	RCP8.5	RCP4.5	RCP8.5
Annual	1.1	1.4	1.6	2.2	2.0	4.1
Winter	1.4	1.4	1.6	2.6	2.3	4.7
Monsoon	1	1.1	1.6	2.2	2.1	3.6
Regional mean annual temperature						
Tibet	1.2	1.6	1.7	2.3	1.9	4.3
High Himalaya	0.8	1.1	1.3	1.9	1.9	3.9
Lower Himalaya	0.8	1.1	1.3	1.8	2	3.6

Nepal (see Figure 1) was also analysed and is summarized in Table 3. There is a high-temperature variation among these regions. The average annual temperature in the Tibet, High Himalaya and Lower Himalaya regions during the base period was -3.7 , -0.5 and 14.4°C , respectively.

Table 4 indicates that increase in temperature for each climate scenario is almost same throughout the regions during short-term, with increase in temperature from 0.6 to 1.4°C and 0.8 to 1.8°C considering RCP4.5 and RCP8.5 scenario, respectively. Average temperature is expected to increase up to 1.9°C considering RCP4.5 and up to 2.8°C considering RCP8.5 in the Tibet in mid-century period. However, higher increase in temperature is expected in the Lower Himalaya (1.5 – 2.6°C) considering RCP4.5 and in the Tibet region (3.2 – 5.6°C) considering RCP8.5 in end-of-century period. Ensemble mean (4 GCMs) of absolute change in average temperature compared to base period in the Koshi river basin is shown in Table 5. Higher increase in temperature is projected in the Tibet region compared to High Himalaya and Lower Himalaya regions.

The spatial pattern of absolute change in ensemble mean temperature compared to reference data during

end-of-century period is shown in Figure 6. Figures 6c,d show the ensemble mean of absolute change in temperature during end-of-century considering RCP4.5 and RCP8.5 scenarios, respectively. Higher increase in temperature is expected in Tibet region compared to High Himalaya and Lower Himalaya regions at the end-of-century period.

Present and future average annual temperature values along with their standard deviation for four GCMs selected for RCP4.5 and RCP8.5 considering end-of-century period is shown in Figure 7b. The average annual temperature in base period is 3.6°C . The average annual temperature values in short-term, mid-century and end-of-century periods are 4.7 , 5.2 and 5.6°C , respectively for RCP4.5 scenario and 5.0 , 5.8 and 7.8°C , respectively, for RCP8.5 scenario.

5 | CONCLUSIONS

The GCMs selection is a critical step for climate change impact studies on different sectors. The advanced envelope-based selection approach, which combines the

past-performance approach and the envelope approach, is applied in this research for the selection of representative global climate models for the transboundary Koshi river basin in China and Nepal. Previous studies conducted on climate projections for the Koshi river basin are based on few GCMs and lack multiple criteria to select GCMs. This study addresses the limitations of the previous studies and provides new climatological insights for the region. A systematic approach for the selection of representative GCM runs from a large pool of climate models and downscaling of climate data for the river basin has been used. The precipitation and temperature data are downscaled for short-term, mid-century and end-of-century periods. The findings for short-term periods could be immediately used by the National Planning Commission, Nepal for the forthcoming 5-year Periodic plan. The ensembles of 105 GCM outputs for RCP4.5 and 78 GCM outputs for RCP8.5 show that uncertainty of future climate in the Koshi river basin is large. Based on these ensembles outputs, the change in temperature and precipitation ranges are estimated.

The main outcomes of this research are as follows:

- The GCM selection for a catchment varies with future scenario chosen (RCP4.5 and RCP8.5) as well as future analysis periods (short-term, mid-century and end-of-century periods).
- The changes in temperature and precipitation range from 0.97–3.29°C and – 7.63 to +3.29%, respectively for mid-century for RCP4.5, whereas for RCP8.5, these ranges are 1.59–4.01°C and – 11.51 to +23.98%.
- Similarly, the change in temperature and precipitation ranges from 1.3–4.6°C and – 9.1 to +31.4%, respectively for end-of-century considering RCP4.5, whereas, for RCP8.5, these ranges are 3.3–7.0°C and – 11.0 to +63.0%.
- However, winter precipitation is projected to decrease in the future. The pre-monsoon precipitation is also expected to decrease in coming decades. Monsoon precipitation is expected to increase in all scenarios and study periods. Similarly, post-monsoon precipitation is also expected to increase in the future.
- Based on the ensemble mean of average precipitation, higher absolute increase in precipitation is expected in Lower Himalaya at short-term period (231 mm for RCP4.5 and 270 mm for RCP8.5) and in High Himalaya region at the mid-century (291 mm for RCP4.5 and 419 mm for RCP8.5) and end-of-century periods (391 mm for RCP4.5 and 922 mm for RCP8.5). Based on the ensemble mean of average temperature, Tibet is more sensitive to climate change considering changes in temperature for all scenarios and study periods. Higher absolute increase in temperature is expected in the Tibet region at short-term (1.2°C for RCP4.5 and 1.6°C for RCP8.5), mid-century (1.7°C for RCP4.5 and 2.3°C for RCP8.5) and end-of-century (1.9°C for RCP4.5 and 4.3°C for RCP8.5) periods compared to the High Himalaya and Lower Himalaya regions.
- Uncertainty in average increase in annual temperature is large in future (1–1.6°C in short-term, 1.3–2.9°C in mid-century and 1.6–5.6°C in end-of-century period).
- Increase in temperature during the winter season is expected to be higher than that in the monsoon period.

Downscaled data (10 × 10 km² grid) for the entire Koshi river basin were developed for each grid point. The downscaled data from the selected GCMs project the following likely future climatic conditions:

- Uncertainty in average increase in annual precipitation is large in the future: 0–16% in short-term, 4–23% in mid-century and 4–24% in end-of-century period, considering the RCP4.5 scenario. Higher uncertainty in precipitation is expected in scenario RCP8.5 as compared to RCP4.5 scenario. The uncertainty in average increase in annual precipitation is 6–20% in short-term, 6–36% in mid-century and 13–49% in end-of-century period, considering RCP8.5 scenario.

The results from this study support the findings from other studies that the temperature and precipitation of the Koshi river basin will most likely follow an increasing trajectory. Similar findings are also suggested for Nepal and the Himalayan region (Agarwal *et al.*, 2014; Agarwal *et al.*, 2016; Nepal, 2016; Wester *et al.*, 2019). Our study also suggests that the selection of models can be very sensitive to the number of parameter (future study periods, ETCCDI indices and seasonal biases) used for a study. The model selected could be different based on different time periods. In the three future time periods we considered, no one model matched in all 3 time periods. This shows that the modified ensemble approach is also very sensitive to the time period chosen.

ACKNOWLEDGEMENTS

The first author, Santosh Kaini, is grateful to Australia Awards Scholarship Program for providing funds for the PhD research at Victoria University, Melbourne. The authors would like to thank Geert Jan van Oldenborgh (Royal Netherlands Meteorological Institute) for making available and assistance with the KNMI Climate Explorer tool. We also thank J. Sillmann and colleagues for making available the output of their analysis on ETCCDI

indices in the CMIP5 multi-model ensemble. We acknowledge the Regional Database System, International Centre for Integrated Mountain Development, Kathmandu, Nepal for making available the precipitation and temperature data for the base period covering the entire Koshi basin. This study was supported by ICIMOD's Kosi Basin Programme which contributes to the Sustainable Development Investment Portfolio and is supported by the Australia aid program.

CONFLICT OF INTEREST

The authors declare that they have no conflict of interest.

ORCID

Santosh Kaini  <https://orcid.org/0000-0002-0991-9334>

REFERENCES

- Agarwal, A., Babel, M.S. and Maskey, S. (2014) Analysis of future precipitation in the Koshi river basin, Nepal. *Journal of Hydrology*, 513, 422–434.
- Agarwal, A., Babel, M.S., Maskey, S., Shrestha, S., Kawasaki, A. and Tripathi, N.K. (2016) Analysis of temperature projections in the Koshi River basin, Nepal. *International Journal of Climatology*, 36, 266–279.
- Bharati, L., Gurung, P., Jayakody, P., Smakhtin, V. and Bhattarai, U. (2014) The projected impact of climate change on water availability and development in the Koshi Basin, Nepal. *Mountain Research and Development*, 34, 118–130.
- Biemans, H., Speelman, L., Ludwig, F., Moors, E., Wiltshire, A., Kumar, P., Gerten, D. and Kabat, P. (2013) Future water resources for food production in five south Asian river basins and potential for adaptation—a modeling study. *Science of the Total Environment*, 468, S117–S131.
- Boé, J., Terray, L., Habets, F. and Martin, E. (2007) Statistical and dynamical downscaling of the Seine basin climate for hydro-meteorological studies. *International Journal of Climatology*, 27, 1643–1655.
- Buytaert, W., Vuille, M., Dewulf, A., Karmalkar, A. and Céleri, R. (2010) Uncertainties in climate change projections and regional downscaling in the tropical Andes: implications for water resources management. *Hydrology and Earth System Sciences*, 14, 1247–1258.
- Chen, S.-T., Yu, P.-S. and Tang, Y.-H. (2010) Statistical downscaling of daily precipitation using support vector machines and multivariate analysis. *Journal of Hydrology*, 385, 13–22.
- Dixit, A., Upadhyaya, M., Dixit, K., Pokhrel, A. and Rai, D.R. (2009) *Living with Water Stress in the Hills of the Koshi Basin, Nepal*. Nepal: International Centre for Integrated Mountain Development.
- Eriksson, M., Xu, J., Shrestha, A.B., Vaidya, R.A., Santosh, N. and Sandström, K. (2009) *The Changing Himalayas: Impact of Climate Change on Water Resources and Livelihoods in the Greater Himalayas*. Nepal: International centre for integrated mountain development (ICIMOD).
- Gleckler, P.J., Taylor, K.E. and Doutriaux, C. (2008) Performance metrics for climate models. *Journal of Geophysical Research: Atmospheres*, 113, 1–20.
- Hong, S.-Y. and Kanamitsu, M. (2014) Dynamical downscaling: fundamental issues from an NWP point of view and recommendations. *Asia-Pacific Journal of Atmospheric Sciences*, 50, 83–104.
- Immerzeel, W.W., Droogers, P., De Jong, S. and Bierkens, M. (2009) Large-scale monitoring of snow cover and runoff simulation in Himalayan river basins using remote sensing. *Remote Sensing of Environment*, 113, 40–49.
- Immerzeel, W.W., Van Beek, L., Konz, M., Shrestha, A. and Bierkens, M. (2012) Hydrological response to climate change in a glacierized catchment in the Himalayas. *Climatic Change*, 110, 721–736.
- IPCC. (2007) *Climate Change 2007: The Physical Science Basis. Contribution of Working Group I to the Fourth Assessment Report of the Intergovernmental Panel on Climate Change*. Cambridge, United Kingdom and New York, NY, USA: Cambridge University Press 996 pp.
- IPCC. (2013) *Climate Change 2013: The Physical Science Basis. Contribution of Working Group I to the Fifth Assessment Report of the Intergovernmental Panel on Climate Change*. Cambridge, United Kingdom and New York, NY, USA: Cambridge University Press 1535 pp.
- IPCC. (2014) *Climate Change 2014: Synthesis Report. Contribution of Working Groups I, II and III to the Fifth Assessment Report of the Intergovernmental Panel on Climate Change*. Geneva, Switzerland: IPCC 151 pp.
- Lee, J., Sperber, K.R., Gleckler, P.J., Bonfils, C.J. and Taylor, K.E. (2019) Quantifying the agreement between observed and simulated extratropical modes of interannual variability. *Climate Dynamics*, 52, 4057–4089.
- Lee, J.-W. and Hong, S.-Y. (2014) Potential for added value to downscaled climate extremes over Korea by increased resolution of a regional climate model. *Theoretical and Applied Climatology*, 117, 667–677.
- Lee, J.-W., Hong, S.-Y., Chang, E.-C., Suh, M.-S. and Kang, H.-S. (2014) Assessment of future climate change over East Asia due to the RCP scenarios downscaled by GRIMs-RMP. *Climate Dynamics*, 42, 733–747.
- Lim, Y.K., Shin, D., Cocke, S., Larow, T., Schoof, J.T., O'Brien, J.J. and Chassignet, E.P. (2007) Dynamically and statistically downscaled seasonal simulations of maximum surface air temperature over the southeastern United States. *Journal of Geophysical Research: Atmospheres*, 112, 1–17.
- Lutz, A. and Immerzeel, W. (2015) Reference climate dataset for the Indus, Ganges and Brahmaputra River basins. In: *Report FutureWater, HI-AWARE Research Component 1*. The Netherlands: HI-AWARE/FutureWater.
- Lutz, A.F., Ter Maat, H.W., Biemans, H., Shrestha, A.B., Wester, P. and Immerzeel, W.W. (2016) Selecting representative climate models for climate change impact studies: an advanced envelope-based selection approach. *International Journal of Climatology*, 36, 3988–4005.
- Maskey, S., Uhlenbrook, S. and Ojha, S. (2011) An analysis of snow cover changes in the Himalayan region using MODIS snow products and in-situ temperature data. *Climatic Change*, 108, 391–400.
- Max-Planck Institute for Meteorology. 2018. *Overview Climate Data Operators*. [Online]. Available: <https://code.mpimet.mpg.de/projects/cdo/> [Accessed 15th August 2018].
- Meehl, G.A., Covey, C., Delworth, T., Latif, M., McAvaney, B., Mitchell, J.F., Stouffer, R.J. and Taylor, K.E. (2007) The WCRP

- CMIP3 multimodel dataset: a new era in climate change research. *Bulletin of the American Meteorological Society*, 88, 1383–1394.
- Nepal, S. (2016) Impacts of climate change on the hydrological regime of the Koshi river basin in the Himalayan region. *Journal of Hydro-Environment Research*, 10, 76–89.
- Nepal, S., Krause, P., Flügel, W.A., Fink, M. and Fischer, C. (2014) Understanding the hydrological system dynamics of a glaciated alpine catchment in the Himalayan region using the J2000 hydrological model. *Hydrological Processes*, 28, 1329–1344.
- Panofsky, H.A. and Brier, G.W. (1968) *Some Applications of Statistics to Meteorology*. University Park: Pennsylvania State University Press Mineral Industries Extension Services, College of Mineral Industries.
- Peterson, T. (2005) Climate change indices. *World Meteorological Organization (WMO) bulletin*, 54, 83–86.
- Pierce, D. W., Barnett, T. P., Santer, B. D. & Gleckler, P. J. 2009. Selecting global climate models for regional climate change studies. *Proceedings of the National Academy of Sciences*, pns. 0900094106.
- Rajbhandari, R., Shrestha, A.B., Nepal, S. and Wahid, S. (2016) Projection of future climate over the Koshi River basin based on CMIP5 GCMs. *Atmospheric and Climate Sciences*, 6, 190–204.
- Rajbhandari, R., Shrestha, A.B., Nepal, S., Wahid, S. and Ren, G.-Y. (2017) Extreme climate projections over the transboundary Koshi River basin using a high resolution regional climate model. *Advances in Climate Change Research*, 8, 199–211.
- Rstudio Team. (2016) *RStudio: Integrated Development for R*. Boston, MA: RStudio, Inc..
- Seager, R., Ting, M., Held, I., Kushnir, Y., Lu, J., Vecchi, G., Huang, H.-P., Harnik, N., Leetmaa, A. and Lau, N.-C. (2007) Model projections of an imminent transition to a more arid climate in southwestern North America. *Science*, 316, 1181–1184.
- Shrestha, A.B. and Aryal, R. (2011) Climate change in Nepal and its impact on Himalayan glaciers. *Regional Environmental Change*, 11, 65–77.
- Sillmann, J., Kharin, V., Zhang, X., Zwiers, F. and Bronaugh, D. (2013a) Climate extremes indices in the CMIP5 multimodel ensemble: part 1. Model evaluation in the present climate. *Journal of Geophysical Research: Atmospheres*, 118, 1716–1733.
- Sillmann, J., Kharin, V., Zwiers, F., Zhang, X. and Bronaugh, D. (2013b) Climate extremes indices in the CMIP5 multimodel ensemble: part 2. Future climate projections. *Journal of Geophysical Research: Atmospheres*, 118, 2473–2493.
- Taylor, K.E., Stouffer, R.J. and Meehl, G.A. (2012) An overview of CMIP5 and the experiment design. *Bulletin of the American Meteorological Society*, 93, 485–498.
- Themeßl, M.J., Gobiet, A. and Heinrich, G. (2012) Empirical-statistical downscaling and error correction of regional climate models and its impact on the climate change signal. *Climatic Change*, 112, 449–468.
- Themeßl, M.J., Gobiet, A. and Leuprecht, A. (2011) Empirical-statistical downscaling and error correction of daily precipitation from regional climate models. *International Journal of Climatology*, 31, 1530–1544.
- Tisseuil, C., Vrac, M., Lek, S. and Wade, A.J. (2010) Statistical downscaling of river flows. *Journal of Hydrology*, 385, 279–291.
- Trzaska, S. and Schnarr, E. (2014) *A review of downscaling methods for climate change projections*. Washington, DC: United States Agency for International Development by Tetra Tech ARD, pp. 1–42.
- Van Vuuren, D.P., Edmonds, J., Kainuma, M., Riahi, K., Thomson, A., Hibbard, K., Hurtt, G.C., Kram, T., Krey, V. and Lamarque, J.-F. (2011a) The representative concentration pathways: an overview. *Climatic Change*, 109, 5–31.
- Van Vuuren, D.P., Stehfest, E., Den Elzen, M.G., Kram, T., Van Vliet, J., Deetman, S., Isaac, M., Goldewijk, K.K., Hof, A. and Beltran, A.M. (2011b) RCP2. 6: exploring the possibility to keep global mean temperature increase below 2°C. *Climatic Change*, 109, 95–116.
- Van Vuuren, D.P., Stehfest, E., Den Elzen, M.G., Van Vliet, J. and Isaac, M. (2010) Exploring IMAGE model scenarios that keep greenhouse gas radiative forcing below 3 W/m² in 2100. *Energy Economics*, 32, 1105–1120.
- Wester, P., Mishra, A., Mukherji, A. and Shrestha, A.B. (2019) *The Hindu Kush Himalaya Assessment—Mountains, Climate Change, Sustainability and People*. Cham: Springer Nature Switzerland AG.
- Willems, P. and Vrac, M. (2011) Statistical precipitation downscaling for small-scale hydrological impact investigations of climate change. *Journal of Hydrology*, 402, 193–205.

SUPPORTING INFORMATION

Additional supporting information may be found online in the Supporting Information section at the end of this article.

How to cite this article: Kaini S, Nepal S, Pradhananga S, Gardner T, Sharma AK. Representative general circulation models selection and downscaling of climate data for the transboundary Koshi river basin in China and Nepal. *Int J Climatol*. 2020;40:4131–4149. <https://doi.org/10.1002/joc.6447>